Peer-reviewed version available at *Appl. Sci.* **2019**, *9*, 4660; doi:10.3390/app9214660

Fragility Assessment of Container Crane under Seismic Excitation Considering Uplift and Derailment Behavior

Quang Huy Tran [1], Jungwon Huh [2,*], Nhu Son Doan [2], Van Ha Mac [2] and Jin-Hee Ahn [3]

[1] Department of Civil Engineering, Nha Trang University, Khanh Hoa, 57000, Vietnam; huytq@ntu.edu.vn (Q.H.T)

[2] Department of Civil and Environmental Engineering, Chonnam National University, Yeosu, 59626, Republic of Korea; 188444@jnu.ac.kr (N.S.D), 188456@jnu.ac.kr (V.H.M)

[3] Department of Civil Engineering, Gyeongnam National University of Science and Technology, Jinju, Gyeongnam 52725, Korea; jhahn@gntech.ac.kr (J-H. Ahn)

* Correspondence: jwonhuh@chonnam.ac.kr; Tel.: +82-61-659-7247

Abstract:

While the container crane is an important part of daily port operations, it has received little attention compared with other infrastructures, such as buildings and bridges. Crane collapse due to earthquake affects the operation of the port, and indirectly impacts the economy. This study proposes fragility analyses for various damage levels of the container crane that allow the port owner and partners to better understand the seismic vulnerability presented by container cranes. A large quantity of nonlinear time history analyses was applied for a three-dimensional (3D) finite element model to quantify the vulnerability of the container crane in considering the uplift and derailment behavior. The uncertainty of demand and capacity of the crane structures were also considered through random variables, i.e. elastic modulus of members, ground motion profile, and intensity. The results analyzed in the case of a Korean container crane showed that the probability of exceeding the first uplift with or without derailment is shown before the crane reaches the structure's limit states. This means that under low seismic excitation, the crane might be derailed without any structural damage. But when the crane reaches the minor damage state, it is always coupled with a certain probability of uplift with or without derailment. This study also proposes the fragility curves developed for different structural periods to enable port stakeholders to assess the risk of their container crane.

Keywords: STS container crane; uplift and derailment; time history analysis; pushover analysis; fragility assessment

Preprints (www.preprints.org) | NOT PEER-REVIEWED | Posted: 15 September 2019 doi:10.20944/preprints201909.0151.v1

Peer-reviewed version available at Appl. Sci. 2019, 9, 4660; doi:10.3390/app9214660

1. Introduction

Container ports in seismically active regions all over the world are vulnerable to severe damage from earthquake. The exposure has considerable economic impact in the affected region. However, container ports generally do not receive similar attention compared with other infrastructure systems, such as buildings, bridges, and water and power plants [1]. One of the most critical but vulnerable components in the operation of a port is the container crane being used for loading and unloading containers from ships. Modern jumbo container cranes may weigh between (1,300 and 1,800) tons. They are capable of lifting containers weighing between (60 and 120) tons to heights between (35 and 42) m above the wharf (or gravity quay wall) [2, 3]. The rail gage/span and portal clearance are designed to adapt to traffic lane widths. A typical portal width is around 30.5 m, and can accept 4 working traffic lanes. Figure 1 shows an example of the Korean A-frame single hoist STS container crane.

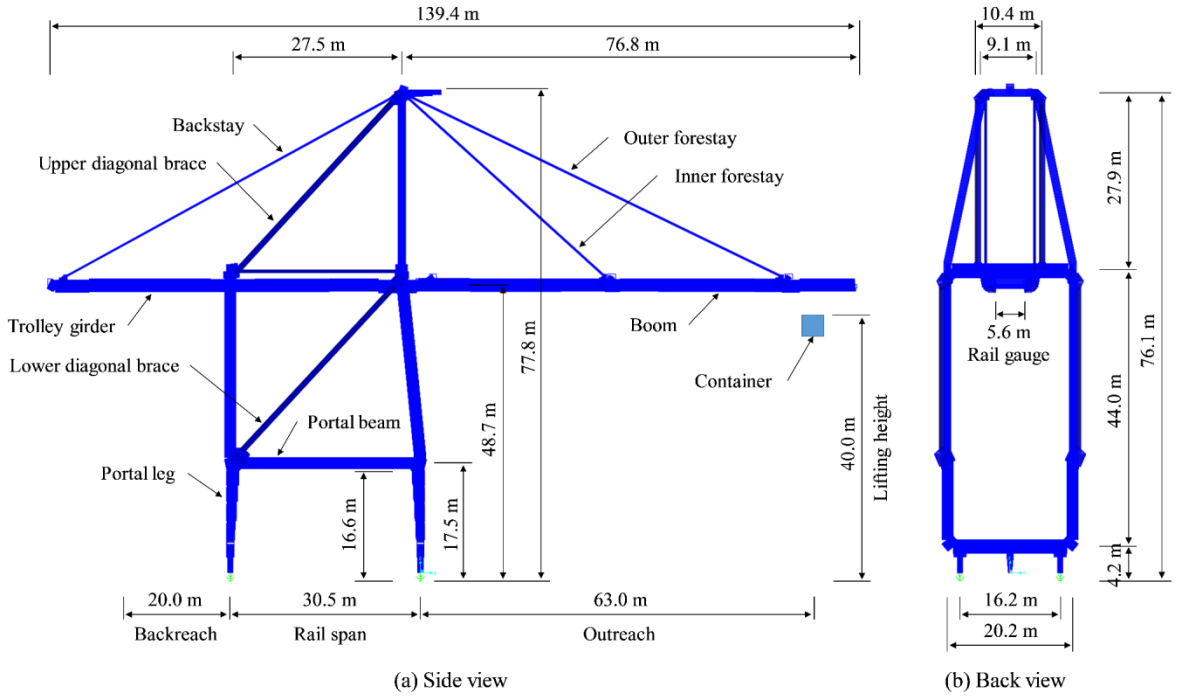

Figure 1. Overall dimensions of the Korean A-frame container crane.

In South Korea, the seismic performance of the container crane has not been considered for most of the port design guidelines in the past, because South Korea was expected to be less severely affected by earthquakes. However, strong shaking occurred recently, i.e. the 5.4

Peer-reviewed version available at Appl. Sci. 2019, 9, 4660; doi:10.3390/app9214660

magnitude Pohang earthquake on 15 Nov. 2017 [4], and the 5.8 magnitude Gyeongju earthquake on 12 Dec. 2016 [5], which damaged several buildings, port facilities, roads, and bridges. Thus, seismic analysis for a container crane needs to be considered more than ever, to reduce the economic and human losses due to earthquake.

Historically, many ports have been partially destroyed by earthquake, e.g. the port of Kobe (Japan) in 1995 [6], the port in Port-au-Prince (Haiti) in 2010 [1], or the port in Chile in 1985 [7], requiring a long time for repair and recovery. In the case of a container crane totally collapsing, it typically takes (12 to 24) months to purchase a new port crane [8]; thus, pre-defined damage levels and structural performance are necessary in the seismic performance evaluation for both new and existing cranes to predict their risks. Fragility analysis is known as a key input parameter for the seismic risk assessment of a structural component or whole system, and allows an evaluation of the potential damage thresholds and specific repair models of a structural component in the system during a predefined intensity earthquake [1]. The fragility curve, which is usually assumed as a cumulative distribution function (CDF) [9], was first applied to civil infrastructures in ATC-13 in the mid-1980s [10], and was later applied to many types of structures, such as bridges [11, 12], highways [13], buildings [14], tunnels [15, 16], and ports [1, 17]. Fragility assessment for the container crane has not been widely studied. A significant study was conducted by Kosbab et al. [1, 18]. Three two-dimensional (2D) numerical models of American cranes, i.e. J100, LD100, and LD50, were considered with overall limit states obtained in terms of critical portal deformations. Based on previous experimental and numerical studies, the hysteretic rotational springs were utilized to capture both elastic and inelastic behavioral features. In addition to the earthquake excitation, fragility assessment due to stochastic wind loading was also considered for container cranes [19].

In this study, a three-dimensional (3D) finite element (FE) model of a typical Korean container crane was used in the fragility analyses. The damage or limit states were defined in terms of portal drift using nonlinear static analysis with hinges defined in compliance with ASCE/SEI 41 [20]. Nonlinear time history analyses were applied with gradually increasing the earthquake intensity (*IM*). A set of twenty recorded and artificial ground motions per IM were matched to the Korean design response spectra [21]. The contacts between the crane's toes and the wharf/rails were simulated by isolator elements of SAP2000, which allow capture of the uplift and derailment behavior. This paper is structured as follows: Section 2 introduces the methodology for the analytical fragility analysis, which covers its procedure to obtain the

Peer-reviewed version available at Appl. Sci. 2019, 9, 4660; doi:10.3390/app9214660

research goal. Section 3 describes the time history analyses on the 3D numerical model to develop the fragility curves. Section 4 presents the results of the analyses, and discusses the performance-based fragility curves. Finally, Section 5 concludes the paper.

2. Analytical Fragility

2.1. Methodology of Fragility Assessment

Fragility analyses, also known as fragility curves, are the representations of conditional probability that indicate the probability of exceeding a pre-defined level of damage as subjected to an input seismic intensity parameter [12]. The fragility function represents the ability of a system to withstand a specified event, and can be expressed as:

$$Fragility = P\left[LS \mid IM = x \right], \tag{1}$$

where, $P[LS|IM = x]$ represents the probability that a ground motion with $IM = x$ causes the structure to collapse with a given pre-defined limit state (LS). The IM can be expressed in terms of peak ground acceleration/velocity/displacement or spectral acceleration at the fundamental period [9]. There are commonly four methods for fragility assessment: (1) professional judgement; (2) quasi-static and design code consistent analysis; (3) the damage data associated with past earthquakes (so-called empirical fragility analysis); and (4) numerical simulation of seismic response based on structural dynamic analysis or so-called analytical fragility analysis [22]. In the absence of adequate damage data, the empirical fragility curve will be inaccurate. Thus, the analytical fragility analysis in which the limit states are defined based on ASCE/SEI 41 [20] for steel building structure can be a suitable tool for assessing the container crane. The definition of limit states is discussed in detail in Part 2.3.

Increasing IM levels have been generated to cover a whole range of each fragility curve. For each IM level, twenty ground motions created by matching the IM level with the design response spectra of the Korean Building Code (KBC) [23, 21] were used as input parameters for the FE model. The time history analyses were carried out to obtain the critical portal drift. Figure 2 illustrates the framework of this study.

Preprints (www.preprints.org) | NOT PEER-REVIEWED | Posted: 15 September 2019 doi:10.20944/preprints201909.0151.v1

Peer-reviewed version available at Appl. Sci. 2019, 9, 4660; doi:10.3390/app9214660

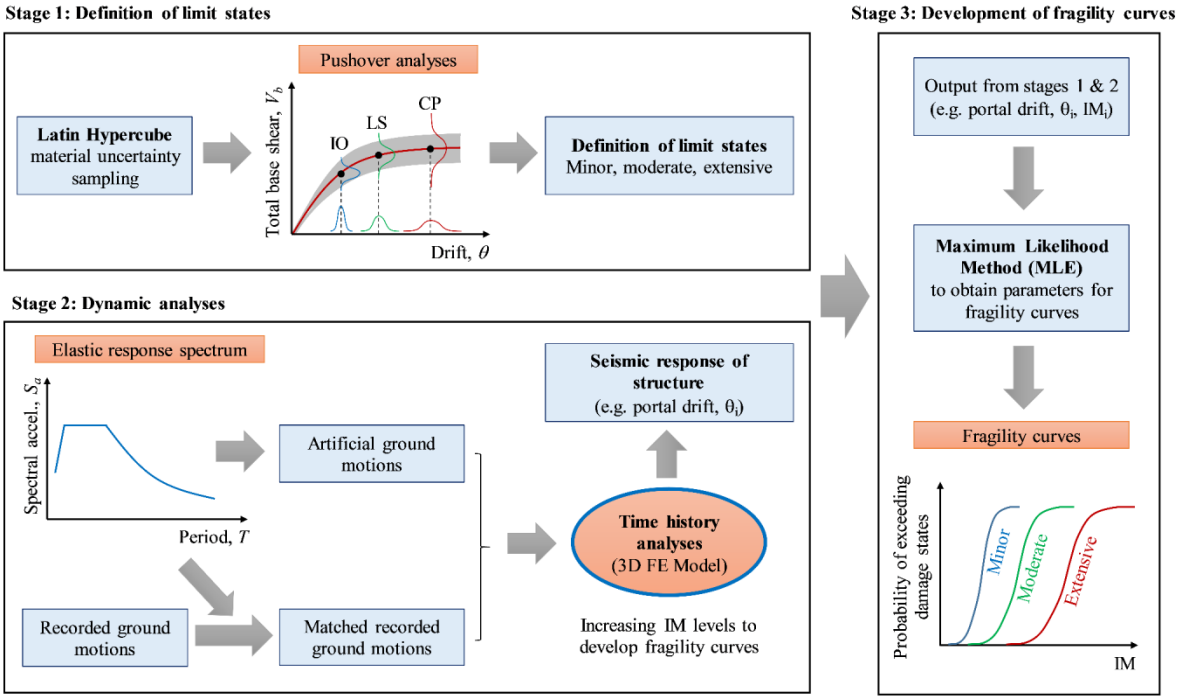

Figure 2. Methodology of fragility curve development.

2.2. Selection of Seismic Demands

Based on the authors' previous study [24], the sensitivity of a crane structure was studied and used for identifying which sources of uncertainty are significant to the response of the structure. A series of random variables, including ground motion intensity, ground motion profiles, mass, damping, and the elastic modulus of steel, were considered. The results showed that of all the sources of uncertainty considered, the ground motion intensity and profile play the most important role in the overall response of the container crane in terms of portal drift. In addition, the elastic modulus is recommended to be considered as a source of uncertainty in the seismic analysis. Thus, to minimize the computational cost, the ground motion intensity and profile are considered as the demand randomness and the elastic modulus of steel is taken into account as the capacity randomness of the container crane. Other uncertain parameters in the finite element analysis are evaluated to be deterministic at their mean/median value.

To consider the site conditions where the crane is located, many boreholes were drilled to investigate some major physical characteristic of the ground, especially the shear wave velocity (v_s) of the top 30 m from the ground surface. The report showed that the minimum and

Peer-reviewed version available at Appl. Sci. 2019, 9, 4660; doi:10.3390/app9214660

maximum of v_s are around (247 and 447) m/s, respectively, indicating that the soil classes ranged from (S2 to S3) according to the KBC, as shown in Table 1:

Table 1. Site classification (Soil classes) of the Korea Building Code [21].

Soil classes	Name of ground type	Classification criteria	
		Bedrock Depth, H (m)	Soil average shear wave velocity, v_s (m/s)
S1	Rock	Less than 1	≥ 760
S2	Shallow and hard ground	(1 – 20 or less)	≥ 260
S3	Shallow and soft ground		< 260
S4	Deep and hard ground	Above 20	≥ 180
S5	Deep and soft ground		< 180 ($v_s \leq 120$ m/s is not classified as S5, regardless of the bedrock depth)
S6	Grounds that require site-specific characterization and ground response analysis		

For the crane's site, seismic zone I (with the seismic zone factor of $Z = 0.11 \times g$) was considered. With a return period of 500 years as recommended for port structures with the assumption that the crane works under the immediate occupancy (IO) performance level [23], and the chosen soil class S3, the 1.5 % damping horizontal acceleration response spectrum was developed, as illustrated in Fig. 3 (a).

Ten recorded ground motions (denoted as RGM) were selected to consider the effect of the realistic ground motion profile, as shown in Table 2; and then a spectrum matching process was conducted to the design response spectrum illustrated in Fig. 3 (b), to generate ten design spectrum-matched ground motions, as shown in Fig. 4 (a). The reason for using the spectrum matching technique is to reduce the variability (jaggedness) observed in the acceleration spectra for individual ground motions [25].

To have the ground motions with a number of peaks of similar amplitude, ten artificial ground motions (denoted as AGM) were generated based on the prescribed response spectrum of Fig. 3 (a) as well. The QuakeGem program was used [26], which is dependent on the spectral-representation-based simulation algorithm proposed by Deodatis in 1996 [27, 28], with filtered white noise signal by three different trapezoidal envelope functions, and Fig. 4 (b) shows ten artificial time history accelerations.

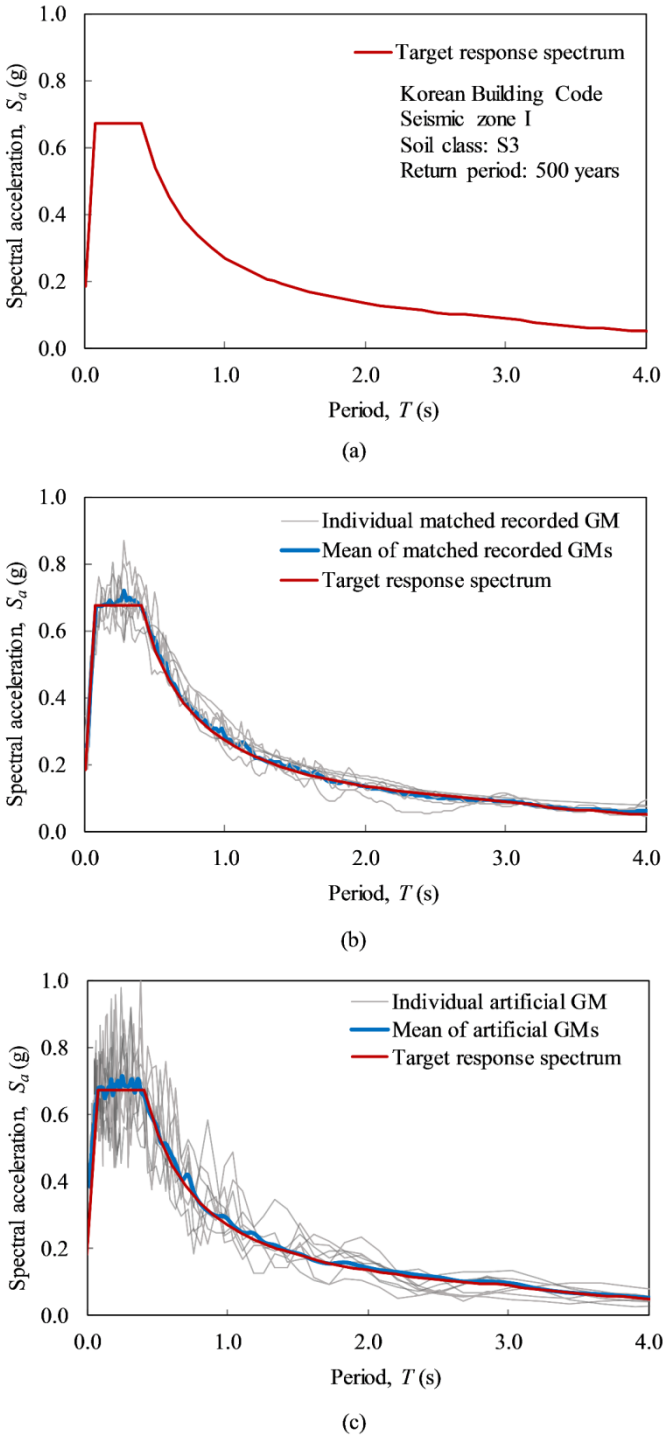

Figure 3. (a) Target response spectrum (1.5 % damping), (b) Matched recorded response spectra, and (c) Artificial response spectra.

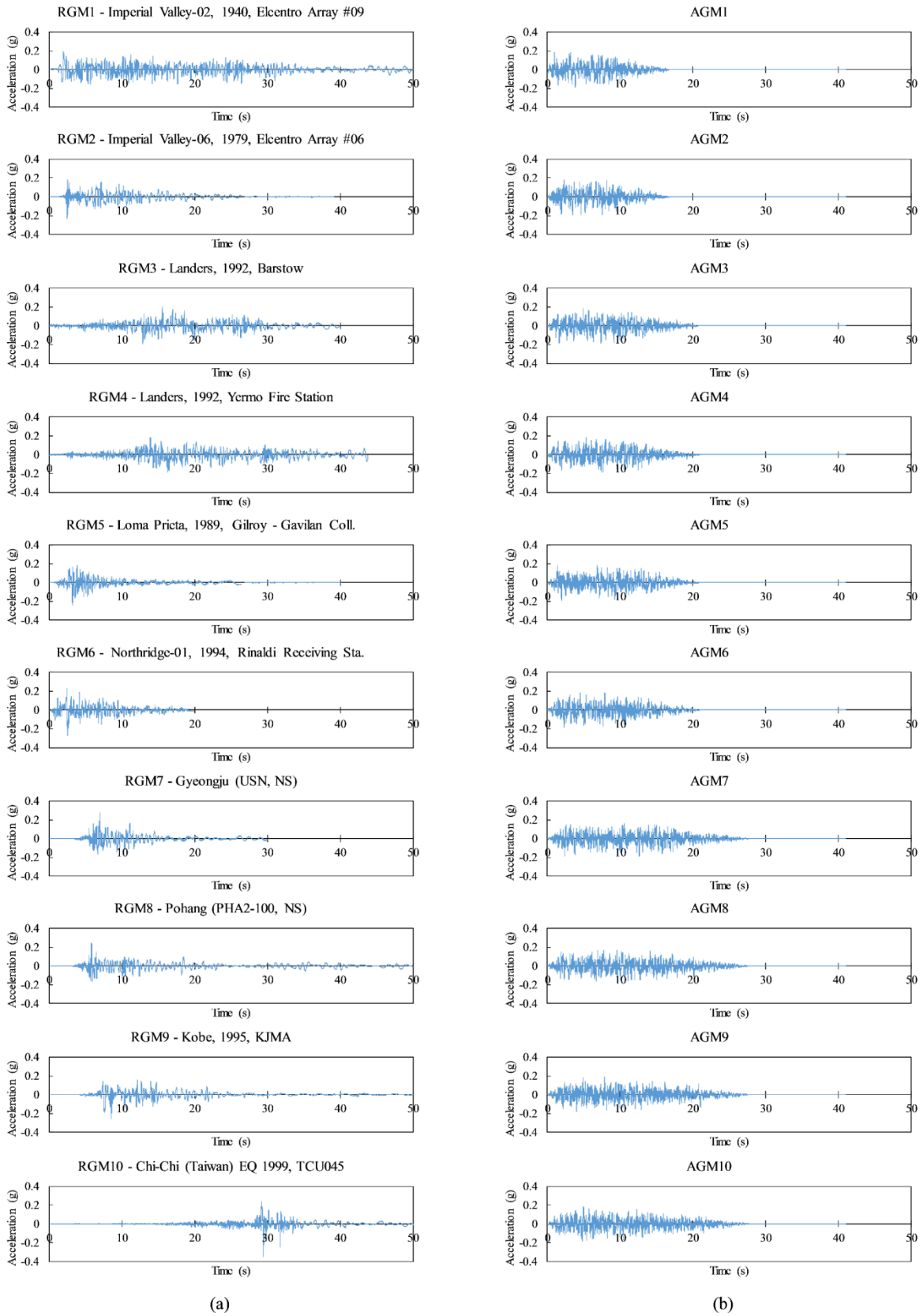

Figure 4. (a) Matched recorded ground motions, and (b) Artificial ground motions.

Peer-reviewed version available at Appl. Sci. 2019, 9, 4660; doi:10.3390/app9214660

Table 2. Original recorded ground motions (unmatched).

GM.	Earthquake name	Year	Station name, direction	Magnitude	PGA (× *g*)
1	Imperial Valley-02	1940	Elcentro Array #09	6.95	0.21
2	Imperial Valley-06	1979	Elcentro Array #06	6.53	0.45
3	Landers	1992	Barstow	7.28	0.13
4	Landers	1992	Yermo Fire Sta.	7.28	0.24
5	Loma Prieta	1989	Gilroy-Gavilan Coll.	6.93	0.36
6	Northridge-01	1994	Rinaldi Receiving Sta.	6.69	0.87
7	Gyeongju, S. Korea	2016	USN, NS	5.80	0.43
8	Pohang, S. Korea	2017	PHA2-100, NS	5.40	0.27
9	Kobe, Japan	1995	KJMA	6.90	0.83
10	Chi-Chi, Taiwan	1999	TCU045	7.62	0.36

2.3. Damage States for Container Crane

For the randomness in a structural capacity, the uncertainty of the overall stiffness of the structure might mainly come from the structure's dimension and material property. In this study, with the assumption that the steel plates were perfectly manufactured, the elastic modulus is the only factor to be considered as a normal distribution random variable with a mean value of 200 GPa and coefficient of variation (COV) of 0.06, respectively [24]. A nonlinear static analysis is then performed to discover the capacity behind the elastic states. The limit states obtained by a pin-based pushover can be applied for comparison with the response obtained from the dynamic analysis, because the capacity of the structure is independent of the loading [1]. The force-displacement curve is obtained by gradually increasing the lateral force assigned at the boom level of the crane. This approach was conducted successfully in the authors' previous study [29], but all the input parameters were used in the previous study as best estimates (mean/median values), without considering the uncertainty of the input values to the response of the structure.

To assess the uncertainty in the input value of the structural capacity, fifty input cases of the elastic modulus values were generated by Latin Hypercube Sampling (LHS), to reduce the computational effort as compared to Monte Carlo Simulation (MCS) sampling, because of the

Preprints (www.preprints.org) | NOT PEER-REVIEWED | Posted: 15 September 2019 doi:10.20944/preprints201909.0151.v1

Peer-reviewed version available at Appl. Sci. 2019, 9, 4660; doi:10.3390/app9214660

stratified technique for the input probability distributions of the LHS method [30]. Correspondingly, fifty different pushover analyses were conducted to identify limit states of the damages based on pre-defined plastic hinges of ASCE/SEI 41 [20]. The three pre-defined performance-based damage levels of the ASCE/SEI 41, i.e. immediate occupancy (IO), life safety (LS), and collapse prevention (CP), are assumed as minor, moderate, and extensive damage states, respectively, in terms of the portal drift of the container crane, as shown in Fig. 5, while Table 3 summarizes the corresponding average values. Note that Table 3 would be useful for the preliminary design of a 30.5 m-gage container crane. For example, if an elastic state is expected for designing a 30.5 m-gage crane with structural similarity, its portal drift, defined as the drift angle between the leg base and the portal beam (see Fig. 1), should be less than the minor state of Table 3. The values shown in Table 3 will be an important factor to develop the fragility curves.

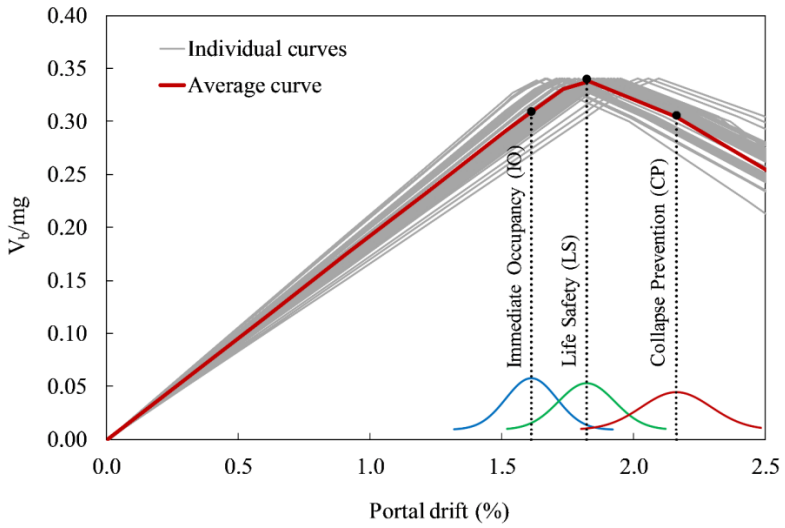

Figure 5. (a) Pushover curves for the fifty random cases generated by Latin Hypercube sampling.

Table 3. Limit states in terms of portal drift

Limit states	Minor	Moderate	Extensive
Portal drift (%)	1.61	1.82	2.16

3. Dynamic Analysis of Container crane coupled with Uplift and Derailment

Peer-reviewed version available at Appl. Sci. 2019, 9, 4660; doi:10.3390/app9214660

3.1. Nonlinear Time History Analyses

In this study, the direct integration nonlinear time history analysis was used, in which the Hilber-Hughes-Taylor (HHT) method was applied to improve numerical dissipation for the time integration algorithm. The parameters of the HHT method are $\gamma = 0.5$, $\beta = 0.25$, and $\alpha = 0$ (accepting that the formulation will be identical to the average acceleration method) [31, 32].

To develop the fragility curves, total of 20 recorded and artificial ground motions matched for the design spectrum as mentioned in Section 2.2 were used under 23 IM levels ranging (0.17 to 0.75)× g. Thus, 460 ground motions were applied as input data for the seismic demand. The *IM* of this research is the spectral acceleration at the fundamental natural period of the container crane, S_a (T = 1.68 s). The fundamental period of this study (applied friction isolator element at the base) is found to be longer than those obtained from our previous studies using the pin-support and gap element [24, 29]. Zero-length link elements of SAP2000 (or friction isolator element) were assigned to the model's toes to simulate the contact friction, allowing both uplift and derailment, because the behavior of these elements is similar to the real interaction between the crane wheel and the rail during the operation of the crane. The uplift and derailment behaviors will change the horizontal displacement of the whole structure; thus the corresponding fragility curves would be different from those obtained from other boundary conditions, such as pin or gap element [29, 33]. Based on both physical test and analytical model of the previous studies, the seismic response of the container crane over time can be divided into three stages [1, 6, 34], as shown in Fig. 6: (a) the structure is shaken due to low seismic load, so-called swaying; (b) with higher seismic load, the landside legs are uplifted and derailed (lateral translation) when the total gravity load is transferred to the waterside legs, due to the considerable reduction of the axial load on the landside legs. As a result, when the load is added on the waterside legs due to the uplift of the landside legs [1], plastic hinges could occur on the waterside legs; and finally (c) the landside legs land inside the rail, resulting in a residual inward displacement of each leg. In this stage, plastic hinges may also be developed on the landside legs. The first occurrence of a plastic hinge can be at either the waterside or landside legs, which might depend on the design strength of the portal frame, the ground motion profile and intensity, the direction of the earthquake, or the friction between the ground/rails and the crane wheels.

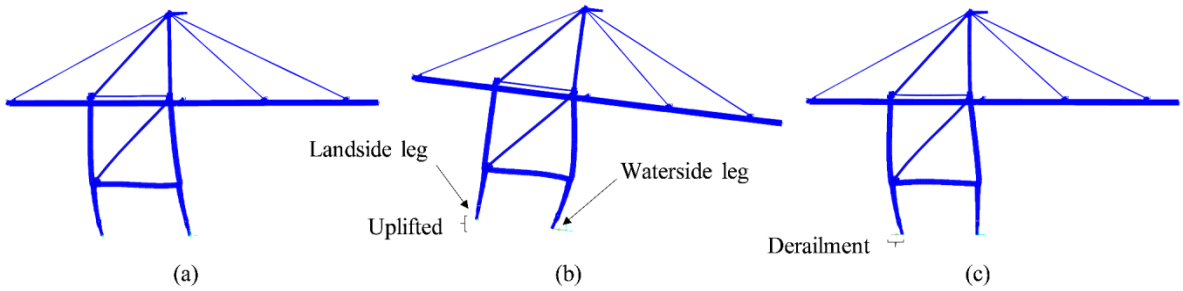

Figure 6. Failure modes of the container crane under the seismic loading; (a) Swaying (b) Uplifted legs with/without derailment, and (c) Permanent derailment and remained deformation.

Figure 7 shows an example of the seismic response of a crane subjected to the artificial ground motion (AGM8) with *PGA* of 0.51 g (equivalent to a scale factor of 3.0 compared to the AGM8 shown in Fig. 4 (b)), considering both the uplift and derailment behaviors. There are four times of uplift at the landside leg. The first uplift occurs at 3.24 s, then reaching its maximum value of 0.04 cm at 3.3 s, and concurrently, it is derailed by as much as 10.4 cm inward at the rail. The second, third, and fourth occurrences of the maximum uplifts are (0.5, 0.1, and 0.9) cm at (4.93, 6.94, and 8.64) s, corresponding to the total permanent derailments of (34.5, 39.2, and 52.0) cm, respectively. In this study, the uplift behavior relates to the redistribution of the load. The uplift is defined by two conditions as mentioned in Tran et al. [29], in which both vertical displacement and the reaction of the uplifted leg are equal to or larger than zero. In particular, Fig. 7 (b) shows four times of uplifting, corresponding to four times of vertical reaction reduced to zero in Fig. 7 (c). Both waterside legs and one landside leg of the crane of this example have drifted over the limit state of collapse prevention, indicating a potential overturning collapse towards the sea. It is noted that the analyses of this study ignore the lateral restraint provided by a small flange on each wheel. Thus, the derailment is controlled by the weight of the crane, and the friction between the crane's toes and the ground/rail.

Preprints (www.preprints.org) | NOT PEER-REVIEWED | Posted: 15 September 2019 doi:10.20944/preprints201909.0151.v1

Peer-reviewed version available at Appl. Sci. 2019, 9, 4660; doi:10.3390/app9214660

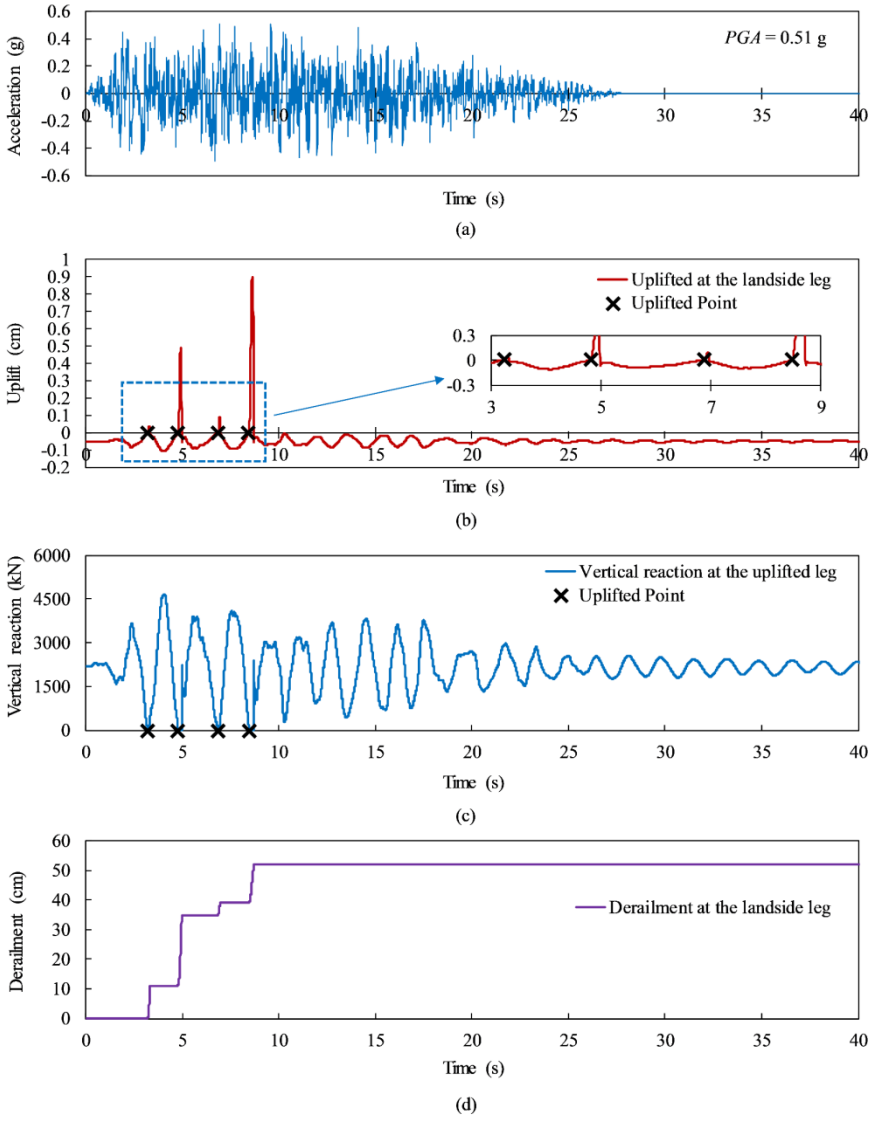

Figure 7. An example of uplift and derailment behaviors of the container crane subjected to the AGM2; (a) Ground motion with *PGA* of 0.51× *g*, (b) Uplift of landside legs, (c) Vertical reaction of landside legs at the time of uplifting, and (d) Derailment of landside legs.

3.2. Probability of Exceedance of Uplift

Based on the above-mentioned definition of an uplift behavior, uplift and derailment are considered to be an independent limit state, because they can occur with or without structural damage. This will be discussed in detail when the uplift curve is considered together with the IO, LS, and CP curves in the following sections. The fragility curve of excessive uplift was

Peer-reviewed version available at Appl. Sci. 2019, 9, 4660; doi:10.3390/app9214660

constructed as the principle of Eq. (1), and detailed in Section 4. Fourteen IM levels were generated ranging (0.17 to 0.61)× g, in which each IM level illustrated as a blue dot in Fig. 8 includes 20 different ground motions. The probability of exceeding uplift under different IM levels was fitted by a log-normal CDF depicted as the red solid line in Fig. 8. The median and standard deviation of ln(IM) are (0.31 and 0.248)× g, respectively.

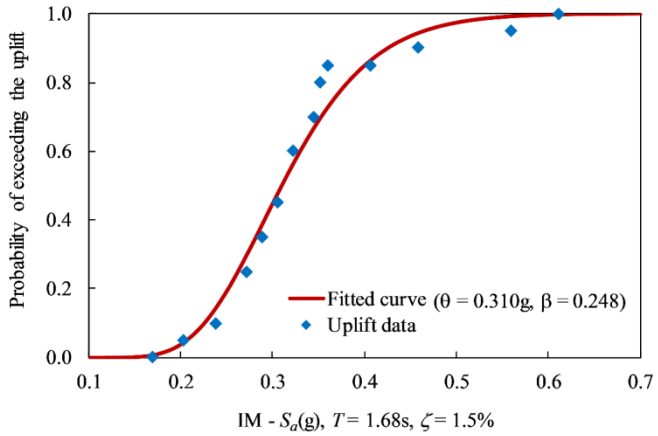

Figure 8. Probability of exceeding the uplift.

4. Performance-based Fragility Curves

As mentioned previously, the log-normal CDF is used to define the fragility function [9, 35, 36], thus, Eq. (1) can be expressed as follows:

$$P(LS \mid IM = x) = \Phi\left(\frac{\ln(x/\theta)}{\beta}\right), \quad (2)$$

where, $\Phi(\,)$ is the standard normal cumulative distribution function, and θ and β are the median and standard deviation of ln(IM), respectively. At each $IM = x_j$, the structural analyses produce some number of collapses out of the total number of ground motions. The probability of observing collapses or no collapses is given by the binomial distribution. Hence, the MLE function is:

Preprints (www.preprints.org) | NOT PEER-REVIEWED | Posted: 15 September 2019 doi:10.20944/preprints201909.0151.v1

Peer-reviewed version available at Appl. Sci. 2019, 9, 4660; doi:10.3390/app9214660

$$Likelihood = \prod_{j=1}^{m} \binom{n_j}{z_j} p_j^{z_j} \left(1 - p_j^{z_j}\right)^{n_j - z_j}, \quad (3)$$

where, p_j represents the probability that a ground motion with $IM = x_j$ causes the collapse, z_j is the number of collapses out of n_j ground motions, and m represents the number of IM level. In order to perform this maximization, Eq. (2) is substituted into Eq. (3), so the fragility parameters are explicit in the likelihood function:

$$Likelihood = \prod_{j=1}^{m} \binom{n_j}{z_j} \Phi\left(\frac{\ln\left(x_j / \theta\right)}{\beta}\right)^{z_j} \left(1 - \Phi\left(\frac{\ln\left(x_j / \theta\right)}{\beta}\right)\right)^{n_j - z_j}, \quad (4)$$

The parameters that maximize this likelihood function also maximize the log of the likelihood. The "$\hat{}$" notation denotes an estimate of a parameter:

$$\left\{\hat{\theta}, \hat{\beta}\right\} = \arg\max \sum_{j=1}^{m} \left\{ \ln\binom{n_j}{z_j} + z_j \ln \Phi\left(\frac{\ln\left(x_j / \theta\right)}{\beta}\right) + \left(n_j - z_j\right) \ln\left(1 - \Phi\left(\frac{\ln\left(x_j / \theta\right)}{\beta}\right)\right) \right\}, \quad (5)$$

Figure 9 shows the three fragility curves built from the definition of Table 3. As a result, the median values of *IM* (in terms of *PGA*) were (0.487, 0.521, and 0.557)× *g* for the minor, moderate, and extensive limit states, respectively. Correspondingly, the standard deviations of ln(*PGA*) were (0.232, 0.235, and 0.240)× *g* for the minor, moderate, and extensive states, respectively. To consider the *IM* in terms of spectral acceleration at the period *T* of 1.68 s and damping ratio ζ of 1.5 %, the median values of S_a were (0.387, 0.413, and 0.442)× *g* for the minor, moderate, and extensive states, corresponding to the log-standard deviations of (0.232, 0.235, and 0.240)× *g*. The standard deviations indicate the slope of the fragility curves, and also increase as the performance levels shift from minor to extensive damage state.

When the uplift coupled with derailment happens, the crane will be repositioned and its functionality restored after landing inside the rails. The failure can occur before or after the uplift threshold, depending on the capacity of each crane. In this analysis, the failure occurs after the uplift threshold; thus the probabilities of exceeding IO, LS, and CP performance levels

Peer-reviewed version available at Appl. Sci. 2019, 9, 4660; doi:10.3390/app9214660

have to be considered coupled with the uplift and derailment behavior, as shown in Fig. 10. At the same *IM* level, e.g. at S_a = 0.387× g, it can be clearly seen that the 50 % probability of exceeding the IO level will be coupled with around 80 % probability of exceeding uplift. Similarly, the 50 % probability of exceeding LS (S_a = 0.413× g) and CP (S_a = 0.442× g) levels will occur with approximately (85 and 90) % probability of uplift, respectively.

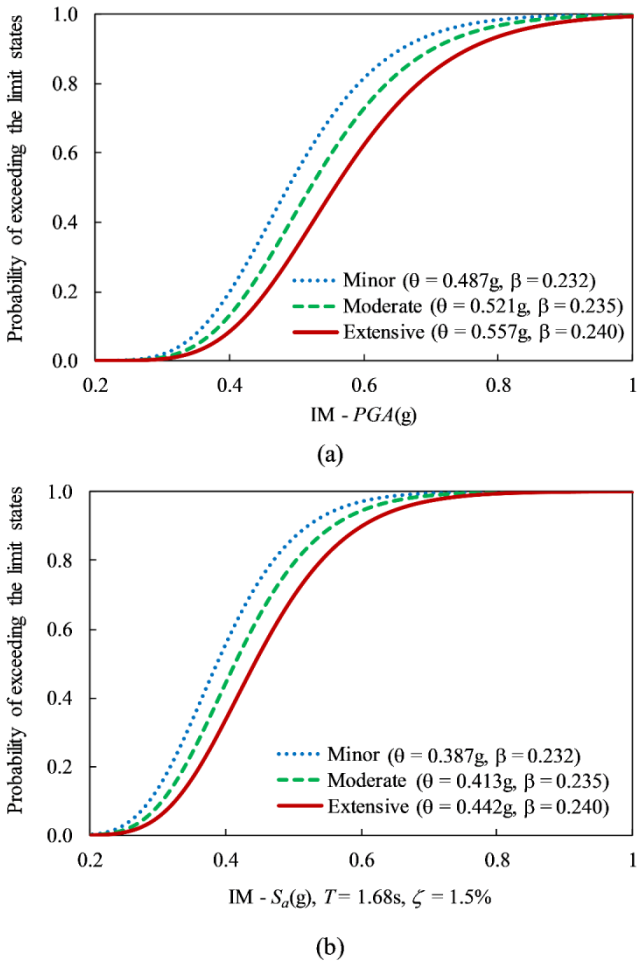

Figure 9. Fragility curves for the minor, moderate, and extensive limit states; (a) IM is the *PGA*, and (b) IM is the S_a (T = 1.68 s, ζ = 1.5 %).

Peer-reviewed version available at Appl. Sci. 2019, 9, 4660; doi:10.3390/app9214660

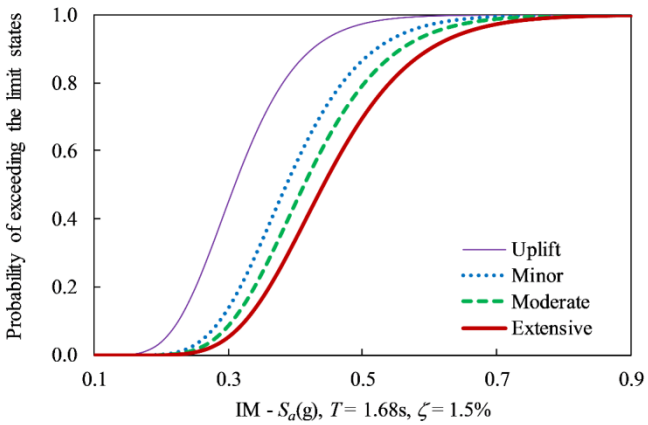

Figure 10. Fragility curves for the uplift, minor, moderate, and extensive limit states.

Based on the proposed fragility curves as shown in Figs. 9 and 10, the vulnerability assessment can be predicted as an example in Table 4 for five different expected seismic levels, with the structure of 1.5 % damping located on the soil S3. The values presented in Table 4 are the probabilities of exceeding damage levels for (200, 500, 1,000, 2,400, and 4,800) average years of return period for the earthquake, equivalent to 10 % probability of occurrence within (20, 50, 100, 250, and 500) years of the structure, as recommended in the KBC. Table 4 can be an essential recommendation for the port owners who want to select a suitable level of risk for their existing cranes, and an appropriate retrofit plan if the cranes suffer an earthquake event in the future. For example, if the owners expect a minor performance level with the seismic Level I for their existing cranes at a Korean port [23], and the selected return period of an earthquake is 500 years, the probability of exceeding minor damage to the crane structures or facilities is around 16 % under the average spectral acceleration S_a of 0.16× g, approximately. Simultaneously, the probability of exceedance of an uplift is around 27 %. On the other hand, assuming the earthquake with a return period of 200 years, the probability of exceeding the minor damage of structure is just around 12 %. However, the business can be interrupted due to 22 % probability of uplift with derailment, because of the operational downtime for jacking and repositioning of the wheels of the crane back to the rail.

Peer-reviewed version available at Appl. Sci. 2019, 9, 4660; doi:10.3390/app9214660

Table 4. An example of the probability of exceeding damage levels (unit %) for five design seismic levels (soil S3) of Korean port design requirements.

Performance levels \ Years of the return period	200	500	1,000	2,400	4,800
Uplift coupled with/without derailment	22	27	35	48	59
Minor	12	16	23	35	46
Moderate	10	14	20	31	42
Extensive	9	12	17	27	38

Figure 11 shows the fragility curves that have been plotted out with four different natural periods of the crane to serve as preliminary design, and to estimate the probability of exceedance for an expected limit state. Based on Fig. 11, the designers or port owners can predict the probability of exceeding limit states for container cranes by a linear interpolation for the fundamental periods ranging (0.5 to 2.0) s. Table 5 shows the parameters of these fragility curve models. It is assumed that the standard deviation of $\ln(S_a)$ is similar to those obtained from Section 4, see Fig. 9 as well.

Table 5. Median and Standard deviation of $\ln(S_a)$.

T (s)	Parameters of fragility curve	IO	LS	CP
0.5	Median	1.277	1.364	1.459
	Standard Deviation	0.232	0.235	0.240
1.0	Median	0.657	0.702	0.751
	Standard Deviation	0.232	0.235	0.240
1.5	Median	0.426	0.455	0.487
	Standard Deviation	0.232	0.235	0.240
2.0	Median	0.320	0.342	0.365
	Standard Deviation	0.232	0.235	0.240

Preprints (www.preprints.org) | NOT PEER-REVIEWED | Posted: 15 September 2019 doi:10.20944/preprints201909.0151.v1

Peer-reviewed version available at Appl. Sci. 2019, 9, 4660; doi:10.3390/app9214660

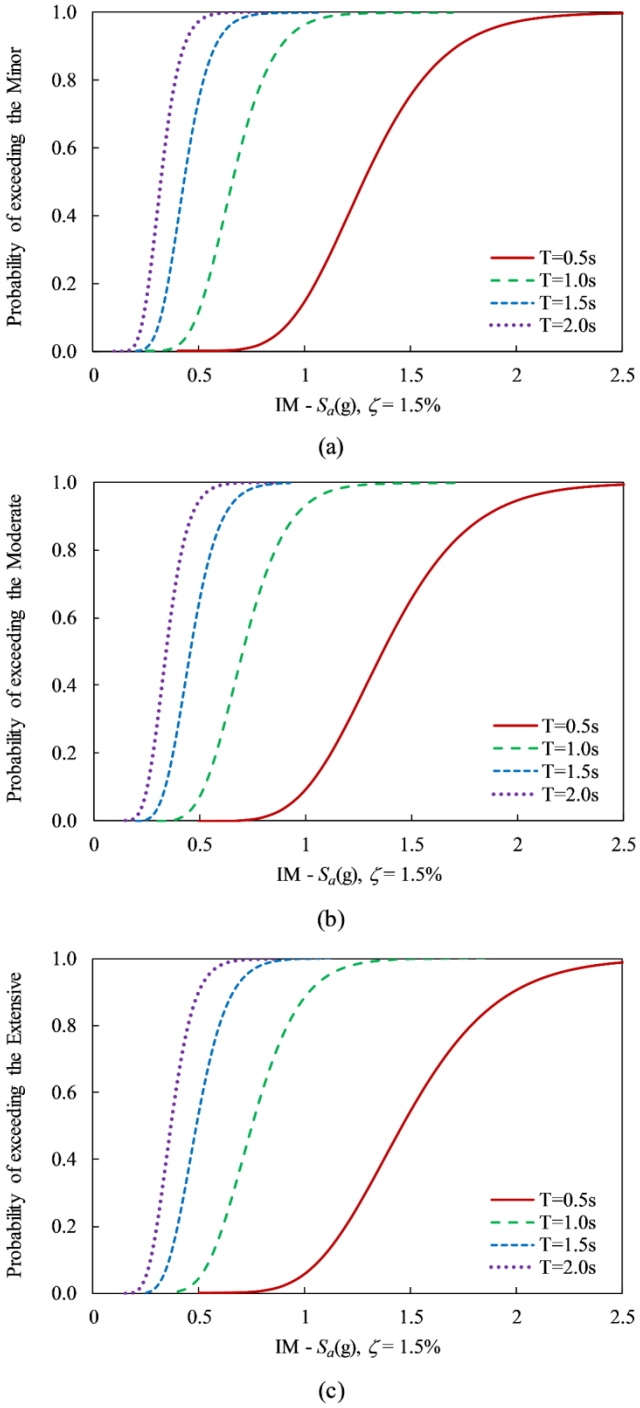

Figure 11. Fragility curves with different periods of container crane for (a) Minor damage state, (b) Moderate damage state, and (c) Extensive damage state.

Peer-reviewed version available at Appl. Sci. 2019, 9, 4660; doi:10.3390/app9214660

5. Conclusions

This study focuses on the time history acceleration analysis of a typical modern jumbo container crane, as well as the methodology in fragility curve development. The methodology can be applied to predicting the probability of exceedance of limit states, based on the pre-defined damage criteria obtained from the combination of the pushover analysis and Latin Hypercube sampling. In addition, the uplift behavior coupled with derailment, which indicates the realistic interaction between the crane toes and the ground/rails, was studied in detail to construct the corresponding fragility curves. The uncertainties of both demand and capacity of the structure were considered, including the elastic modulus, ground motion profile, and intensity.

In this study, the uplift occurs before other damage states. For the container crane of this study, 50 % probability of exceeding the minor damage state will be coupled with around 80 % probability of excessive uplift. Similarly, 50 % probability of exceeding the moderate and extensive damage level will happen with approximately (85 and 90) % probability of uplift, respectively. The longer the natural period of a container crane, the higher the probability of occurrence of the uplift coupled with derailment. This will lead to interruption to the business, due to operational downtime for jacking and repositioning the crane back to the rail. This study also provides the fragility curves that have been developed with different structural natural periods to serve for port stakeholders/designers to consider the risk of their container crane with an expected performance level.

Acknowledgments

This research was a part of the project entitled ‘Development of performance-based seismic design technologies for advancement in design codes for port structures’, funded by the Ministry of Oceans and Fisheries, Korea; and was also supported by the Basic Science Research Program through the National Research Foundation of Korea (NRF), funded by the Ministry of Education (2017R1D1A3B03032854).

Conflicts of Interest: The authors declare no conflict of interest.

Peer-reviewed version available at Appl. Sci. 2019, 9, 4660; doi:10.3390/app9214660

References

[1] Kosbab B.D., "Seismic Performance Evaluation of Port Container Cranes Allowed to Uplift," Georgia Institute of Technology, May 2010.

[2] E. Soderberg, J. Hsieh and A. Dix, "Seismic Guidelines for Container Cranes," in *TCLEE 2009: Lifeline Earthquake Engineering in a Multihazard Environment*, Oakland, California, United States, June 28-July 1, 2009.

[3] Bhimani A. and Jordan M.A., "A few facts about jumbo cranes," in *TOC Americas in Panama*, December 3, 2003.

[4] H.-H. Kim, J.-H. Ree, Y. Kim, S. Kim, S.-Y. Kang and W. Seo, "Assessing whether the 2017 Mw 5.4 Pohang earthquake in South Korea was an induced event," *Science*, vol. 360, no. 6392, pp. 1007-1009, 1 June 2018.

[5] S.-K. Kim and J.-M. Lee, "Probabilistic seismic hazard analysis using a synthetic earthquake catalog: comparison of the Gyeongju City Hall site with the Seoul City Hall site in Korea," *Geosciences Journal*, vol. 21, no. 4, pp. 523-533, 2017.

[6] T. Kanayama and A. Kashiwazaki, "An Evaluation of Uplifting Behavior of Container Cranes Under Strong Earthquakes (in Japanese)," *Transactions of The Japan Society of Mechanical Engineers*, vol. 64, no. 618, pp. 100-106, 1998.

[7] PIANC, Seismic Desing Guidelines for Port Structures, A.A. Balkema, 2001.

[8] M. Vuojolainen and J. Van Der Waal, "A longer lift for your port cranes," Kalmar, Helsinki, Finland, 2015.

[9] Baker J.W., "Efficient analytical fragility function fitting using dynamic structural analysis," *Earthquake Spectra*, vol. 31, no. 1, p. 579, 2015.

[10] ATC-13, Earthquake Damage Evaluation Data for California, Redwood City, CA: FEMA, 1985.

[11] M. Shinozuka, M. Q. Feng, H.-K. Kim and S.-H. Kim, "Nonlinear static procedure for fragility curve development," *Journal of Engineering Mechanics*, vol. 126, no. 12, pp. 1287-1295, Dec. 2000.

[12] J. E. Padgett and R. DesRoches, "Methodology for the development of analytical fragility curves for retrofitted bridges," *Earthquake Engng Struct. Dyn.*, vol. 37, p. 1157–1174, 2008.

[13] K. Pitilakis, "D3.7 Fragility functions for roadway system elements," Norwegian Geotechnical Institute (NGI), 2011.

[14] S. K. Ramamoorthy, P. Gardoni and J. M. Bracci, "Probabilistic Demand Models and Fragility Curves for Reinforced Concrete Frames," *Journal of Structural Engineering*, vol. 132, no. 10, p. 1563, October 2006.

[15] J. Huh, Q. H. Tran, A. Haldar, I. Park and J.-H. Ahn, "Seismic Vulnerability Assessment of a Shallow Two-Story Underground RC Box Structure," *Appl. Sci.*, vol. 7, no. 7, p. 735, 2017.

[16] Argyroudis S.A. and Pitilakis K.D., "Seismic fragility curves of shallow tunnels in alluvial deposits," *Soil Dynamics and Earthquake Engineering*, vol. 35, pp. 1-12, April 2012.

[17] H. Heidary-Torkamani, K. Bargi, R. Amirabadi and N. J. McCllough, "Fragility estimation and sensitivity analysis of an idealized pile-supported wharf with batter piles," *Soil Dynamics and Earthquake Engineering*, Vols. 61-62, pp. 92-106, 2014.

[18] B. Kosbab, R. DesRoches and R. Leon, "Seismic Fragility of Jumbo Port Container Cranes," in *12th Triannual International Conference on Ports*, Jacksonville, Florida, United States, April 25-28, 2010.

[19] S. Gur and S. Ray-Chaudhuri, "Vulnerability assessment of container cranes under stochastic wind loading," *Structure and Infrastructure Engineering*, vol. 10, no. 12, p. 1511–1530, 2014.

[20] ASCE/SEI 41, "Seismic Evaluation and Retrofit of Existing Buildings," American Society of Civil Engineers, Reston, VA, 2013.

[21] Architectural Institute of Korea, "Korean Building Code," Seoul, 2016.

[22] M Shinozuka, M.Q. Feng, H. Kim, T. Uzawa and T. Ueda, "Statistical Analysis of Fragility Curves," University of Southern California, Los Angeles, California, 2001.

[23] I. Kim, "Seismic Design and Performance Objectives of Civil Facilities," *The magazine of the KSCE*, vol. 65, no. 4, pp. 20-25, April 2017.

[24] Q. H. Tran, J. Huh, V. B. Nguyen, C. Kang, J.-H. Ahn and I.-J. Park, "Sensitivity Analysis for Ship-to-Shore Container Crane Design," *Applied sciences*, vol. 8, no. 9, p. 1667, 2018.

[25] A. Whittaker, G. Atkinson, J. Baker, J. Bray, D. Grant, R. Hamburger, C. Haselton and P. Somerville, Selecting and Scaling Earthquake Ground Motions for Performing Response-History Analyses, Gaithersburg, MD: Grant/Contract Reports (NISTGCR) - 11-917-15, Nov. 2011.

[26] Kim J.M., QuakeGem - Computer program for generating multiple earthquake motions, Chonnam National University, 2007.

[27] Deodatis G., "Non-stationary Stochastic Vector Processes: Seismic Ground Motion Applications," *Probabilistic Engineering Mechanics*, vol. 11, pp. 149-168, 1996a.

[28] Deodatis G., "Simulation of Ergodic Multivariate Stochastic Processes," *Journal of Engineering Mechanics*, pp. 778-787, 1996b.

[29] Q. H. Tran, J. Huh, V. B. Nguyen, A. Haldar, C. Kang and K. M. Hwang, "Comparative Study of Nonlinear Static and Time-History Analyses of Typical Korean STS Container Cranes," *Advances in Civil Engineering*, Vols. 2018, Article ID 2176894, p. 13 pages, 2018.

[30] R. L. Iman and W. Conover, "Small sample sensitivity analysis techniques for computer models.with an application to risk assessment," *Communications in Statistics - Theory and Methods*, vol. 9, no. 17, pp. 1749-1842, 1980.

[31] E. Wilson, Three-Dimensional Static and Dynamic Analysis of Structures: A Physical Approach With Emphasis on Earthquake Engineering, Berkeley, California, USA: CSI, 2002.

[32] SAP2000, "Linear and Nonlinear Static and Dynamic Analysis and Design of 3D Structures: Basic Analysis Reference Manual," CSI, Berkeley, California, USA, 2006.

[33] J. Huh, V. B. Nguyen, Q. H. Tran, J.-H. Ahn and C. Kang, "Effects of Boundary Condition Models on the Seismic Responses of a Container Crane," *Applied Sciences*, vol. 9, p. 241, 2019.

[34] R. Kourkoulis, F. Gelagoti and M. Loli, "Seismic Vulnerability of Container Cranes: The Role of Soil-Structure Interaction in Jeopardising Their Operability," in *SECED 2015 Conference: Earthquake Risk and Engineering towards a Resilient World*, Cambridge UK, 9-10 July 2015.

[35] Ibarra L.F. and Krawinkler H., "Global Collapse of Frame Structures under Seismic Excitations," PEER Center, 2005.

[36] T.-H. Lee and Mosalam K.M., "Probabilistic Seismic Evaluation of Reinforced Concrete Structural Components and Systems," PEER Center, Univ. of California, Berkeley, 2006.